Chemical Engineering Journal Advances 12 (2022) 100423

Contents lists available at ScienceDirect

Chemical Engineering Journal Advances

journal homepage: www.sciencedirect.com/journal/chemical-engineering-journal-advances

Real-time degradation of methylene blue using bio-inspired superhydrophobic PDMS tube coated with Ta-ZnO composite

Gulshan Verma [a], Monsur Islam [b], Ankur Gupta [a,*]

[a] Department of Mechanical Engineering, Indian Institute of Technology Jodhpur, Rajasthan 342037, India
[b] Institute of Microstructure Technology, Karlsruhe Institute of Technology, Germany

ARTICLE INFO

Keywords:
Superhydrophobic surface
PDMS tubes
Lotus leaf replication
Ta-ZnO composite
Photocatalytic application
Real-time monitoring
MB dye

ABSTRACT

Dyes are widely used in a variety of industrial applications for aesthetical purpose as well as to provide the color of their products. Huge amount of dye-containing wastewater is released after their processing, posing a risk of environmental contamination. This has prompted the development of low-cost, highly reliable, and long-term technologies for effluent remediation. In this work, the synthesized tantalum (Ta)-doped Zinc oxide (ZnO) composite coated over the bioinspired polymeric platform has been reported for the decolouration of methylene blue (MB) dye when exposed to UV light. These structures were carefully investigated using a scanning electron microscope (SEM), energy dispersive X-ray spectroscopy (EDS), X-ray diffraction (XRD), and a contact angle (CA) goniometer. The contact angle results show the contact angle of 108° for pure polydimethylsiloxane (PDMS) and 168° for bio-inspired PDMS with Ta-doped ZnO composite leading to a superhydrophobic surface. This superhydrophobic bio-inspired polymeric platform was modified by optimizing the surface roughness and coating it with low-surface-energy Ta-ZnO NWs composites, paving the way for it to be envisioned in "self-cleaning" water treatment facilities. When exposed to UV light, the MB dye degradation time was reduced from 150 mins to 105 mins, indicating that the synthesized Ta-doped ZnO NWs composite is more effective than ZnO. These photocatalysts lead to "waste control using Ta-ZnO NWs composites," which opens up new possibilities for flexible and biocompatible environmental remediation platforms. In this study, real-time MB dye degradation is also monitored using the Internet of things (IoT) technique by integrating a NodeMCU microcontroller board as a control center and a pH sensor as a tool for detecting the change in pH value of the MB dye under UV light exposure.

1. Introduction

The chemical business makes extensive use of color. However, the usage of paints in industry is rapidly growing, the resulting in increased the natural water contamination. In fact, even extremely little level of dye in the water (as little as 1 mgL^{-1} for certain dyes) is visible and enough to cause esthetic issues. Organic chemicals, such as dyes, are toxic to humans [1]. It is believed that about 15% of all dyes produced in the world are discarded in the dying and printing operations, and this waste is released into the water. As a result, innovative wastewater treatment technologies are always needed to address environmental contamination. Traditional techniques for wastewater decontamination have been used for decades, including adsorption, coagulation, the Fenton process, flocculation, aerobic treatment, heterogeneous photocatalysis, reverse osmosis, precipitation, ozonation, membrane filtration, and many more [2]. These traditional technologies, however, are inefficient in wastewater treatment and reuse owing to several restrictions such as expensive chemical and operating expenses, advanced processes, complicated sludge production, separation challenges, long process times, and many more. Photocatalysis is a potential approach for eliminating organic pollutants without producing secondary pollutants that require additional treatment. Different metal oxide semiconductors are thought to be potential photocatalysts such as ZnO, TiO_2, SnO_2, WO_3, etc., for converting organic pollutants to ecologically favorable species [3–8]. Because of its photosensitivity, nontoxicity, and lower price than precursors, ZnO is a potential semiconductor for photocatalytic applications [9]. The wide bandgap and higher recombination rate of photoexcited electron-hole pairs are the major disadvantages that prevent ZnO nanoparticles from being used in industry [10]. A literature analysis also revealed that due to faster electron and hole recombination, undoped ZnO has only limited photocatalytic effectiveness [11]. As a result, some method of slowing recombination and increasing the

* Corresponding author.
E-mail address: ankurgupta@iitj.ac.in (A. Gupta).

https://doi.org/10.1016/j.ceja.2022.100423

Available online 14 November 2022

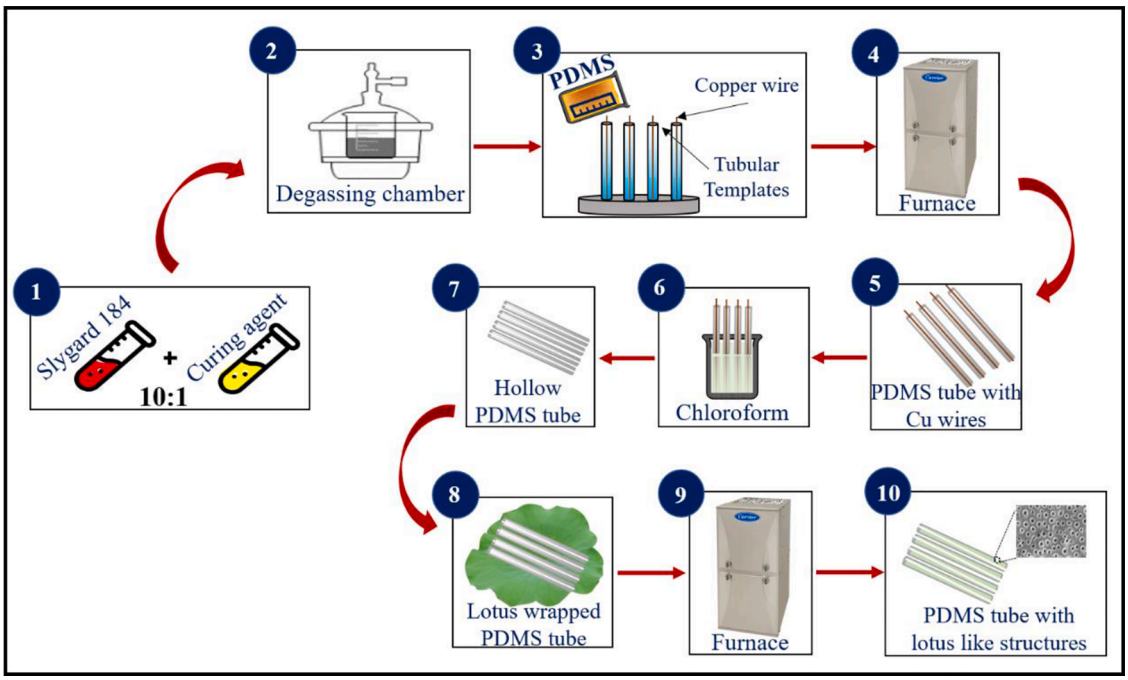

Fig. 1. Schematic of fabrication of hollow PDMS tube with lotus-like microstructures.

number of charge carriers is required. To improve the performance of ZnO, the technique of doping specific appropriate metal ions is used. Transition metals such as Ag, Co, Ce Cu, Cr, Mn, Mo, Ni, Ta, and V, have been doped into ZnO to change their properties [12–14]. Tantalum (Ta) is one of the suitable doping metals for ZnO, with an ionic radius of 0.064 nm (Ta^{5+}) that is similar to that of 0.074 nm (Zn^{2+}). When compared to other transition metals, Ta is the most effective dopant for boosting ZnO photocatalytic ability [15,16]. Most industrial wastewater contains methylene blue (MB), the most prevalent color in effluent from the fabric, sheet, and printing companies. It is difficult to eliminate MB from the wastewater due to the existence of an aromatic ring structure that contains polar groups and chromophores. Many researchers are working to eliminate MB by adsorption by lotus leaves [17].

In recent years, superhydrophobic surfaces having more than 150° water contact angle (WCA) have piqued academic and industrial attention. For many applications, having unique features is crucial such as biocompatibility, self-cleaning, water repellency, improved material durability, and other features to avoid contamination [18]. The chemical composition and morphological features present on a surface are considered to influence super hydrophobicity [19]. In nature, there are a lot of plants that have hydrophobic surfaces. The air was trapped as a cushion for the water droplets that dropped on the leaf due to the hierarchical micro/nanostructures, resulting in superhydrophobicity. In this study, we have attempted to develop lotus leaf-like superhydrophobic structures on polydimethylsiloxane (PDMS) substrate and to examine its photocatalytic ability to degrade MB dye when coated with Ta-ZnO composite. Because of its ductility and biocompatibility, the PDMS substrate is ideal for flexible and stretchable platform [20,21]. Therefore, it has a wide range of applications [22–25]. Industrial wastewater, mostly from chemical and pharmaceutical processing, frequently contains contaminants that must be treated before being discharged. The effect of not adhering to the standard disposal of dyes is that water with an uneven acidity level would disrupt the environment's health and ecology. Manual collection of water samples at various sites is used in traditional water quality procedures, which are then analyzed in laboratories to identify the character of water. The procedure will result in certain errors, such as the worker entering incorrect data. Therefore, in this study, real-time MB dye degradation is monitored using the IoT technique. We have a monitoring system based on the NodeMCU microcontroller development board as a control center and a pH sensor as a tool for detecting the change in pH value of the Textile dye [26]. The first section of this paper discusses the basic introduction

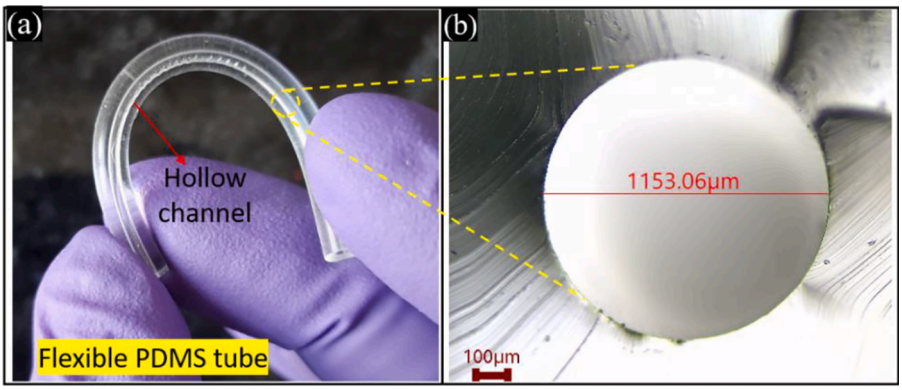

Fig. 2. (a, b) Flexible PDMS tube with an inner diameter of 1.15 mm.

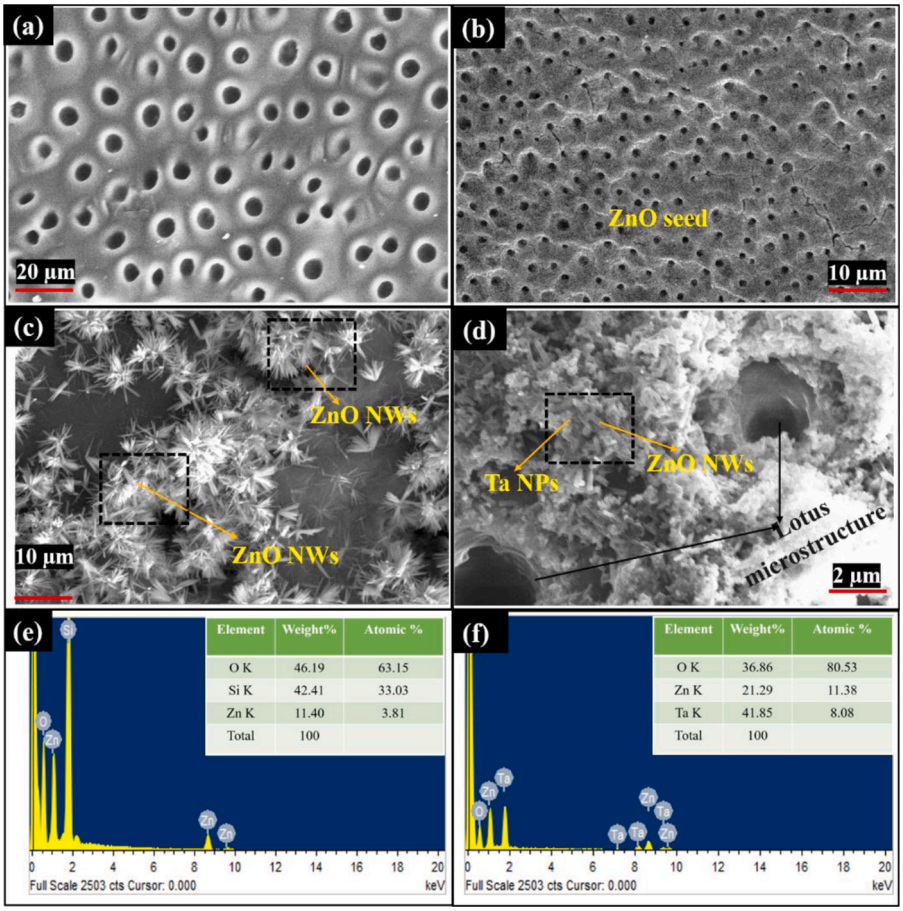

Fig. 3. SEM image of (a) L-PDMS, (b) L-PDMS/ZnO seed layer, (c) L-PDMS/ZnO NWs, and (d) L-PDMS/Ta doped ZnO NWs, and (e-f) EDS results of a sample L-PDMS, and L-PDMS/Ta-doped ZnO.

and requirements for Ta-ZnO composite for photocatalytic applications. The various materials and procedures for preparing PDMS tubes, as well as the synthesis technique used for Ta-ZnO NWs composite are discussed in Section 2. In Section 3, the experimental characterization, result of photocatalytic and real-time degradation are discussed.

2. Materials and methods

Sigma-Aldrich provided zinc acetate dihydrate ($ZnC_4H_6O_4$), potassium hydroxide (KOH), methanol, zinc nitrate, hexamethylenetetramine (HMTA), isopropyl alcohol (IPA), Slygard 184, and curing agent and methylene blue dye. All of the chemicals utilized were AR grade, and they were used exactly as they were received, with no further purification.

2.1. Fabrication of superhydrophobic PDMS tube

The PDMS prepolymer (Slygard 184) and curing agent are mixed in a 20 ml beaker in a 10:1 ratio before being placed in a vacuum desiccator to remove any air bubbles that form during the mixing process (see Fig. 1). After 30 mins of degassing, PDMS is poured into 2 mm diameter plastic tubes which are placed vertically. Now, a copper wire with a diameter of 1.0–1.25 mm is inserted vertically into the PDMS-filled tubular template and cured in an electric oven at 80 °C for 5 hrs. The 2 mm diameter PDMS tubes are then carefully removed from the tubular template. Now, for the removal of copper wire, the whole PDMS tube was dipped in chloroform for 30 s [11]. The chloroform allows PDMS to swell and copper wire will be easily removed by applying a light mechanical pulling force. Finally, the hollow PDMS tube can be obtained. For bio-mimicking the structure of the lotus leaf on PDMS, a fresh lotus leaf is taken and cleaned thoroughly and dried. A thin layer of PDMS is applied over the leaf using a brush, and a fabricated PDMS tube is wrapped around the leaf and placed in an electric oven at 65 °C for 60 mins to cure. Fig. 2 shows the prepared hollow PDMS tube.

2.2. Growth of Ta-Zno composite over the PDMS tubes

The synthesis of Ta-ZnO composite initiates with the seeding on PDMS tubes with ZnO and Ta-ZnO nanoparticles (NPs). For the preparation of Ta-ZnO seed solution, 3 g of $Zn(CH_3COO)_2(H_2O)_2$ were dissolved in 62.5 ml of isopropyl alcohol and 93 mg Ta_2O_5 in 25 ml of glacial acetic acid. Thermal treatment was provided at 100 °C to both solutions after mixing and magnetically agitated for 60 min. Pure ZnO reference samples were simultaneously synthesized using the same procedure but do not contain the Ta_2O_5 precursor. Both the prepared NPs were used to further seed the PDMS tubes.

The prepared PDMS tubes were cleaned with acetone and DI water, then dip-coated in both seed solution one after another, for the initial growth of the ZnO and Ta-ZnO seed layer, and finally calcined at 70 °C in an electric oven. A high-density and the uniform ZnO seed layer is preferred to accelerate the growth of the Ta-ZnO NWs. Now, in a 500 ml beaker, a homogeneous solution containing $Zn(NO_3)_2$ and HMTA (1:5) is prepared in DI water using a probe sonication technique. The ultrasonication technique is used to homogenize the solution. In a separate beaker, a Ta_2O_5 solution was made by dissolving 0.2 g of Ta_2O_5 in 20 ml ethanol and then ultrasonicated for 180 mins. Then, 4 mL of Ta_2O_5 solution was added to the previously prepared $Zn(NO_3)_2$ - HMTA solution. After that, seed PDMS tubes were placed in the solution for 8 hrs at 90

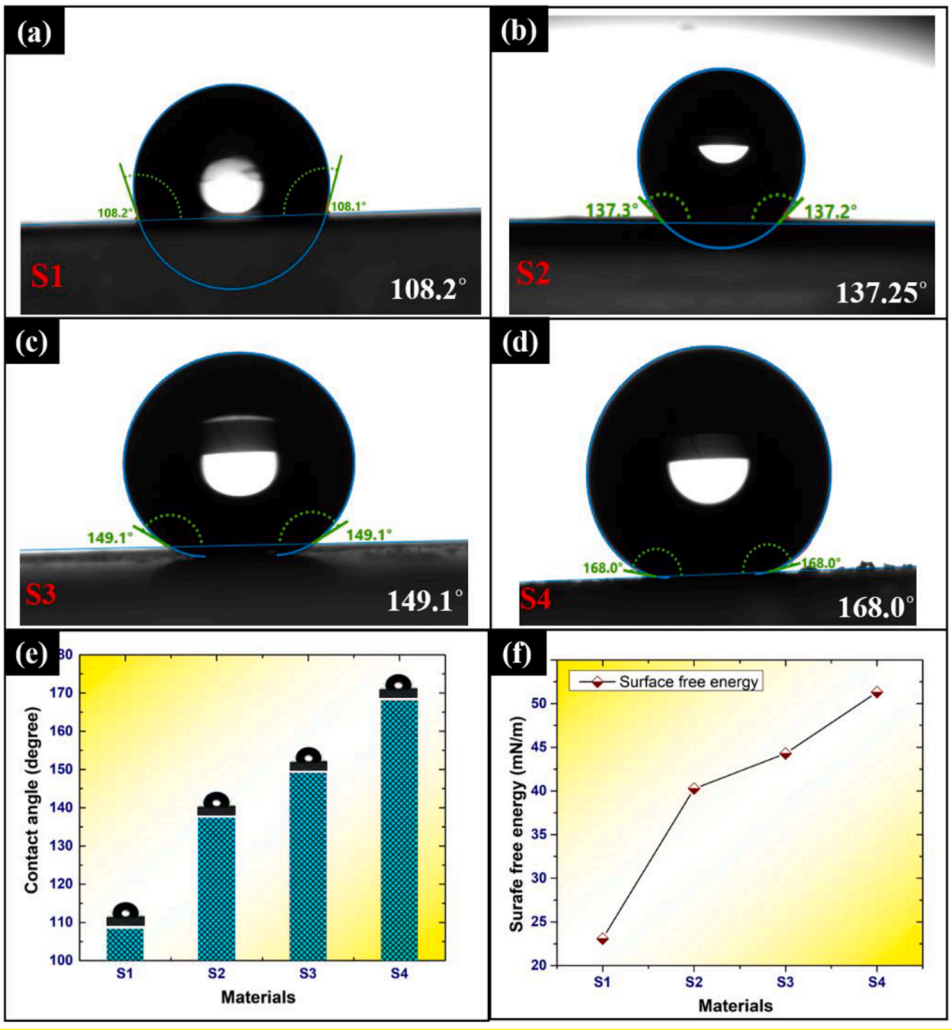

Fig. 4. Contact angle results of (a) S1- pure PDMS (without lotus structure replications (CA: 108.3°)), (b) S2- L-PDMS (CA: 137.25°), (c) S3- L-PDMS/ZnO NWs (CA: 149.1°), and (d) S4- L-PDMS/Ta doped ZnO NWs (CA: 168.1°), and graphical representation of (e-f) CA and SFE.

°C. Finally, the Ta-ZnO composite is deposited on the PDMS tube. Similar technique was used to grow Ta-ZnO nanocomposite using the Ta-ZnO seeded PDMS tubes, but this method led to the agglomeration of nanoparticles and the loss of the nanowire-like structures over the PDMS tubes.

3. Results and discussions

3.1. Surface characteristics

An SEM (Carl Zeiss) and EDS (Oxford instruments) were used to examine the surface morphological features of all the synthesized specimens at an accelerating voltage of 10 kV. The SEM image of (a) lotus microstructure replicated PDMS (L-PDMS), (b) L-PDMS/ZnO seed layer, (c) L-PDMS/ZnO NWs, and (d) Ta-ZnO NWs coated over L-PDMS tube are shown in the Fig. 3 (a-d). The presence of Ta and Zn can be evaluated by EDS results (see Fig. 3e–f). The surface energy of seed layer is high due to its small size. After the substrate is placed in the growth solution, a thin, homogeneous film of finely dispersed seed is attached to the PDMS substrate, enticed Zn^{2+} and O^{2-} ions to the seed, lowering surface energy. These ions have quite enough energy to unify and organize themselves in the ⟨002⟩ to form a hexagonal structure because of the optimal temperature for growth [27]. 1-D polycrystals in the form of NWs were formed as a result. Because of the presence of HMTA, which impedes lateral progression, NWs with finely distributed seeds has enough free space for compact growth of smaller diameters. In addition, the ability of any substrate to support a uniform distribution of nano seeds is linked to the formation of ZnO NWs. The properties of the substrate's surface have a huge influence on the film's deposit that provides growth nucleation sites [28]. The following equations show the growth of ZnO NWs.

$$Zn(NO_3)_2.6H_2O \rightarrow Zn^{2+} + 2NO_3 + 6H_2O \quad (1)$$

$$C_6H_{12}N_4 + 6H_2O \rightarrow 6HCHO + 4NH_3 \quad (2)$$

$$C_6H_{12}N_4 + 4H_2O \rightarrow (CH_2)_6(NH)_4 + 4OH^- \quad (3)$$

$$NH_3 + H_2O \rightarrow OH^- + NH_4^+ \quad (4)$$

$$Zn^{2+} + 4OH^- + H_2O \rightarrow Zn(OH)_4^{2-} \quad (5)$$

$$Zn(OH)_4^{2-} \rightarrow ZnO + H_2O + 2OH^- \quad (6)$$

3.2. Water contact angle (WCA) results

The Kruss DSA25B instrument was used to predict the water contact angle (CA) of pure and Ta-ZnO coated PDMS tubes. The results show that as the Ta-ZnO composite over lotus microstructure-based PDMS tubes grows, the CA increases to 168.0° in comparison to pure PDMS tubes with

Table 1
The characteristics of probe liquid.

Probe Liquid	Polar[#]	SFT[#]	Disperse[#]
Toluene	2.3	28.4	26.1
Water	51	72.8	21.8

[#] mN/m.

a CA: 108.2°. Fig. 4 shows the results of the contact angle of various samples, (a) S1- pure PDMS(without lotus structure replications), (b) S2- L-PDMS, (c) S3- L-PDMS/ZnO NWs, and (d) S4- L-PDMS/Ta doped ZnO NWs. Table 1 shows the properties of probe liquid.

OWRK technology has been used to develop a working model that distinguishes interfacial tensions based on the fundamental interactions between molecules. From the SEM results, the pore size space between the surface of NWs helps capture air, resulting in a decrease in the solid liquid interface, and thus increasing the CA of the Ta-ZnO NWs surface, according to SEM findings.

According to the literature, if the CA is ⟨ 90°, the surface will be sufficiently wet and the liquid will spread over the entire surface, whereas, the surface will be poorly wetted and the liquid reduces its contact with the surface to produce droplets if the CA is ⟩ 90° The greater the CA, the higher the cohesion and the interactions between liquid molecules are frequently more in contrast to those between solid molecules. As a result of the increased CA, the cohesiveness of the Ta-ZnO composite is significantly better than pure ZnO adhesion. Furthermore, the air was trapped as a cushion for the water droplets that dropped on the lotus-like structure with Ta-ZnO NWs composite due to the hierarchical micro/nanostructures, resulting in superhydrophobicity of up to 168°. Fig. 4 (e-f) depicts the graphical relationship between contact angle and material, as well as SFE and material.

3.3. X-ray diffraction (XRD)

Fig. 5 depicts the XRD patterns of ZnO and Ta doped ZnO films. The diffraction patterns were recorded in the 2θ range of 20–80° using Cu K1α radiation (1.54059 Å). The peaks of the hexagonal wurtzite phase of ZnO were identified and peak intensity matches with JCPDS card No. 00–036–1451 [29]. The XRD patterns corresponding to Ta-doped ZnO are shown in Fig. 5b. These patterns have the same characteristics as those found in undoped ZnO samples. After 200° of thermal treatment, we see the presence of the Ta_2O_5 precursor phase. The major peak of this phase is 2Θ=23°. This is similar to the finding reported by Richard et al. [30]. The influence of temperature on the XRD pattern of Ta-doped ZnO was further investigated by the author, who discovered that when the temperature rises, the peak of 2Θ=23° decreases.

3.4. Photocatalytic degradation of Ta-Zno NWs composite grown over PDMS tubes

The photocatalytic efficiency of nanowires generated on the fabricated tubular hollow PDMS substrate was evaluated by analysing the rate of degradation of MB in an aqueous solution with UV radiation. The Fig. 6 shows the schematic diagram of the experimental setup. To expose the Ta-ZnO/PDMS tubes to the 300 mL MB dye solution formed with a 10 mg L-1 (concentration), a small acrylic tank with two holes at the base was formed and the solution was gradually agitated by hand. Periodically take a 3 mL sample of the mixture and record the UV–Vis absorption spectrum to assess the rate of degradation.

The degradation of MB dye based on the exposure to UV light and the effect of Ta-ZnO NWs composite were examined. The maximum peak intensity and position of the MB dye remained at 664 nm, after 105 mins of observation. As time passes, the maximum peak intensity at 664 nm decreases significantly, which is attributed to MB dye degradation, demonstrating that Ta-ZnO NWs composite has strong degradation reactivity against the MB dye (see Fig. 7a-b). Fig. 7(c) depicts a degradation in normalized maximum absorbance as a function of time. According to Beer-Lambert's rule, the concentration and absorbance of an MB dye solution have a linear relationship, and the standardized MB dye concentration replaces the normalized absorbance. Previous studies focus on the kinetic model of Langmuir-Hinshelwood which is useful for explaining the degradation of various dyes. The first-order equations are shown below.

$$-\frac{dB}{dt} = -kB \tag{14}$$

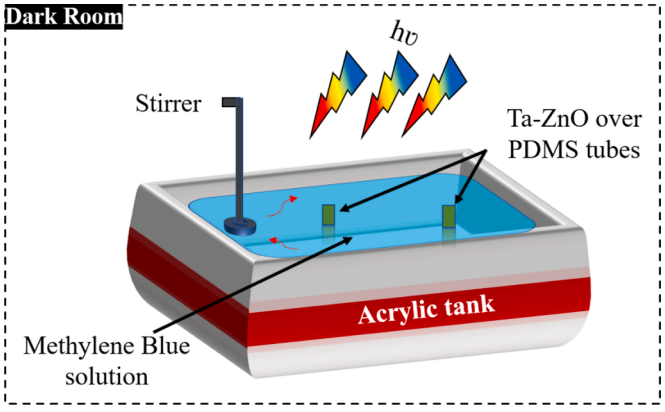

Fig. 6. Schematic representation of photocatalytic degradation setup.

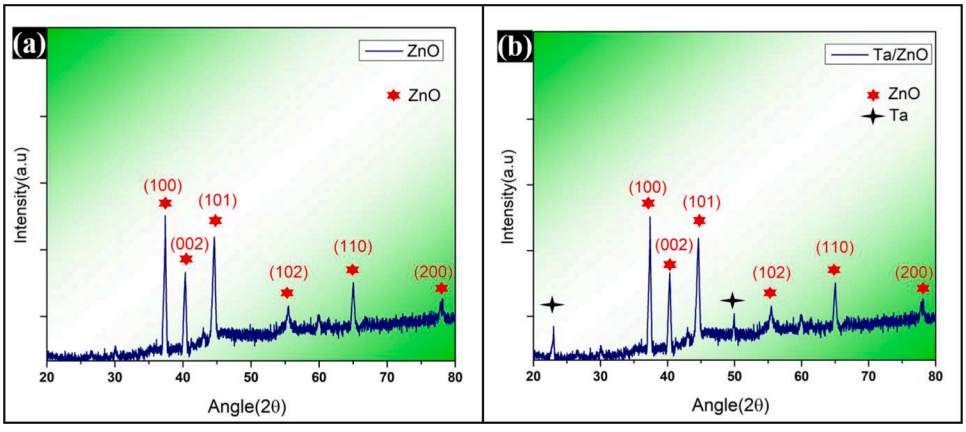

Fig. 5. XRD pattern of (a) ZnO, and (b) Ta-ZnO.

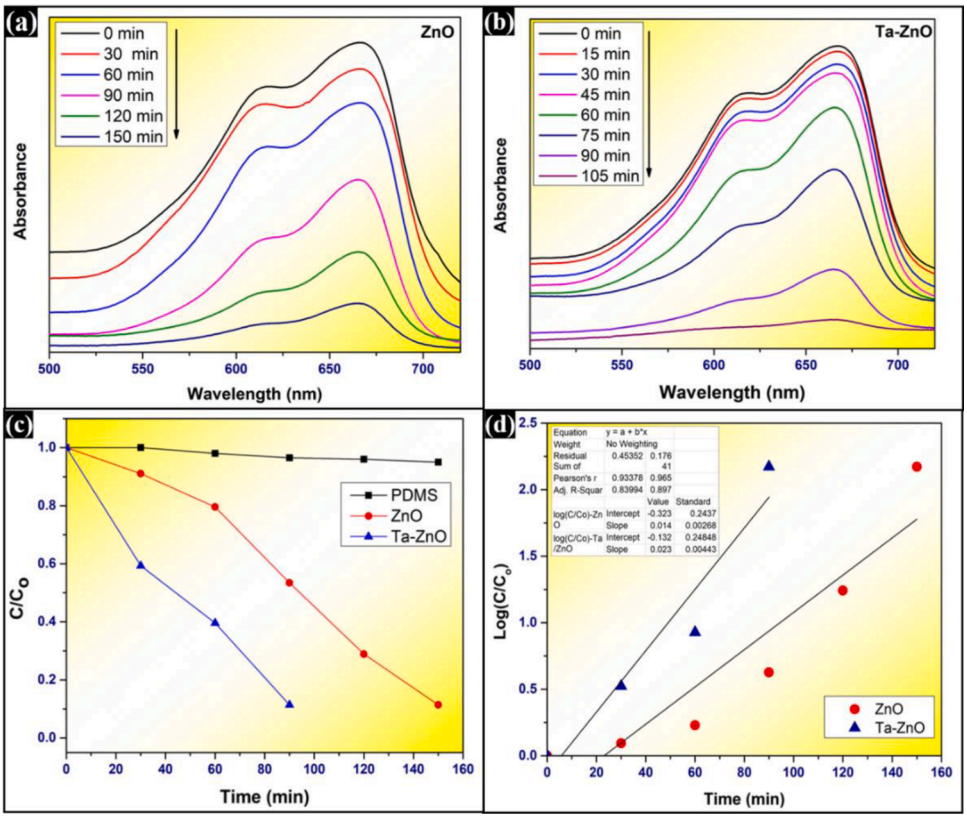

Fig. 7. UV–vis spectrum of (a) pure ZnO, (b) Ta-ZnO composite, and (c, d) experimental and kinetics of photodegradation of MB dye.

$$ln\frac{B}{B_0} = kt + constant \tag{15}$$

Where B_0 and B represent the initial and final concentrations of MB dye, whereas k represents the first-order rate constant calculated from the linear regression kinetics line graph. According to Fig. 7C, the degradation of MB dye pursues pseudo-first-order kinetics. Slope value Ta-ZnO is higher than ZnO, indicating the higher rate constant. The pH sensors were integrated with the electronics circuit to perform real-time MB dye degradation illustrated in Fig. 8.

A pH sensor module (Robocraze) and a NodeMCU ESP8266 microcontroller form the basis of this electronic circuit. The pH sensor data from the MB Dye will be streamed to a web server and made available to the public via IoT on their smartphones (details can be found in the supplemental documentation). A pH sensor uses a potential difference between two electrodes to determine the acidity of water. Small ions enter the borders of the glass membrane when the pH sensor is submerged in an MB dye solution, whereas larger ions remain in the solution. This has the capacity to make a potential difference. The potential difference between electrodes is measured using a pH sensor. It is indeed directly translatable to a pH value. The pH sensor is required to be calibrated in order to obtain accurate results. Standard calibration solutions at pH 4, and pH 7 were used for calibration. The degradation of MB dye by adsorption onto Ta-ZnO composite was found to be slower at first but subsequently became faster as contact duration increased. The degradation of MB dye was found to increase when the pH increased from 6.35 to 6.64 (see Fig. 8A). Similar literature shows, that increasing trends in the pH value of the MB dye solution in response to UV and solar irradiation were also found [31,32].

The degradation characteristics of MB dye molecules on the surface of Ta-ZnO composite are also influenced by the surface charge property of the composite, which is dependent on the pH point of zero charges (pH_{PZC}). The pH_{PZC} of ZnO was 8.5 when determined using the pH drift technique [33]. As a result, the surface of the adsorbent is positive at $(pH)_{MB} < (pH_{PZC})_{Ta\text{-}ZnO}$, resulting in electrostatic repulsion between MB cations and the Ta-ZnO composite. Furthermore, at a pH of 6.35, H^+ ions are present in high concentrations, competing with dye cations for active sites on Ta-ZnO surfaces, resulting in increased substantial MB degradation on the Ta-ZnO composite surface [34,35].

3.5. Reason for enhanced photocatalytic degradation

UV light (366 nm) is absorbed by ZnO-Ta composites, which allows more electrons to be transferred from lower to higher energy levels. The breakdown of MB in an aqueous solution is mostly caused by hydroxyl radical oxidation. In the presence of dissolved$\boldsymbol{O_2}$, photoinduced electrons from Ta-ZnO produces $\boldsymbol{O_2^-}$ (superoxide radicals), which can thereafter form $\boldsymbol{H_2O_2}$ and $\cdot\,\boldsymbol{OH}$ radicals. Because holes have a high oxidation potential, they can cause $\boldsymbol{H_2O}$ to decompose into extremely reactive $-\,\boldsymbol{OH}$ groups. Reactive oxygen vacancies that have been cleaved as electron acceptors briefly block photogenerated electrons, inhibit surface recombination of photogenerated electrons and holes, and then attack dissolved O_2. It results in the formation of $\boldsymbol{O_2^-}$ (superoxide radicals) or $-\,\boldsymbol{OH}$groups on the surface.

The photocatalytic activity of Ta-doped ZnO may be deduced as follows based on the preceding experimental results. (a) For the breakdown of MB dyes, a Ta-doped ZnO composite coated over a PDMS tube serves as an electron and hole source. In ZnO crystals, Ta^{5+}ions play a crucial role in the creation of hole-electron couples. (b) oxygen and hydrogen-related defects aid in the separation of electron-hole pairs and reduce chemical product combination reactions. (c) In photocatalytic activity, the $-\,\boldsymbol{OH}$ groups on the surface also serve as an effective center for the mineralization of organic substances. Higher photocatalytic effectiveness is associated with more surface $-\,\boldsymbol{OH}$ groups.

$$(ZnO-Ta)+h\upsilon\rightarrow(ZnO-Ta)(e^-+h^+) \tag{16}$$

$$\boldsymbol{O_2}+\boldsymbol{e^-}\rightarrow\boldsymbol{O_2^-} \tag{17}$$

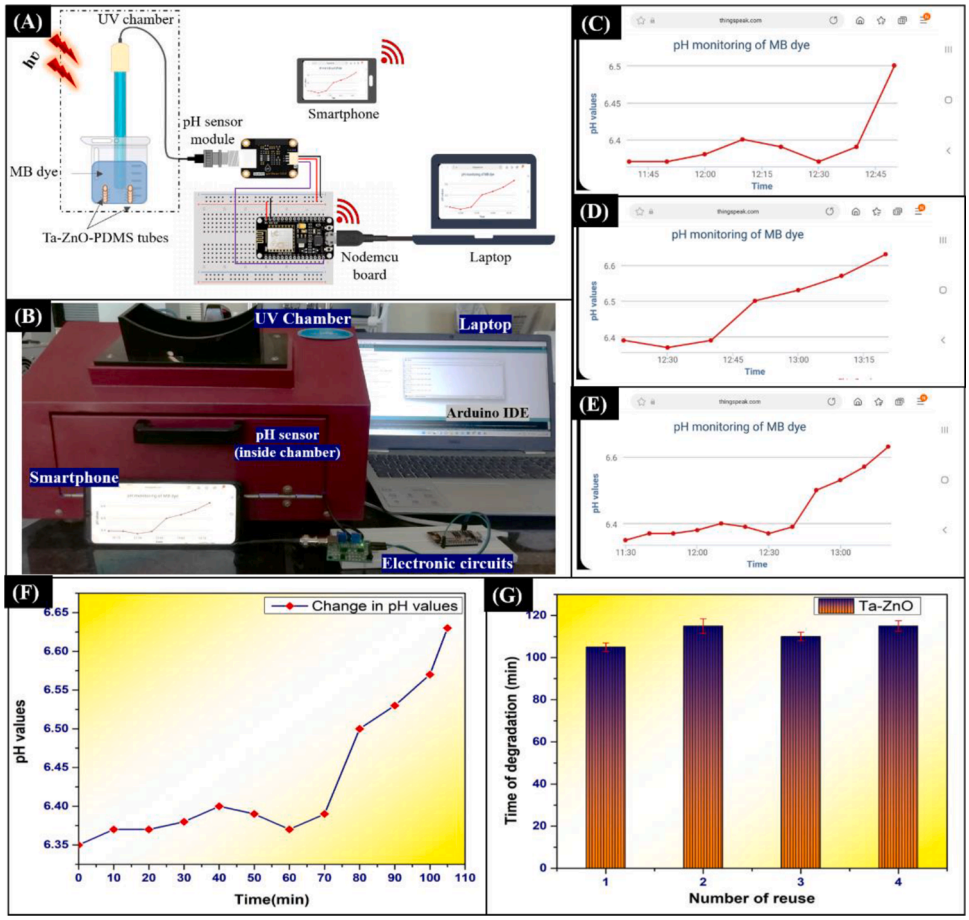

Fig. 8. (A) Schematic representation of real-time pH monitoring of MB dye degradation using NodeMCU and pH sensor module, (B) pictorial representation of experimental setup, (C-E) Real-time pH values monitored in between experiments at different intervals of time (Total time = 105 min), (F) Real-time change in pH values at an interval of 10 min, and (G) repeatability curve.

$$\boldsymbol{O_2^-} + \boldsymbol{e^-} + 2\boldsymbol{H^+} \rightarrow \boldsymbol{H_2O_2} \quad (18)$$

$$H_2O_2 \rightarrow 2\ (\cdot OH) \quad (19)$$

$$h^+ + OH^- \rightarrow \cdot OH \quad (20)$$

$$h^+ + H_2O \rightarrow \cdot OH + H^+ \quad (21)$$

$$\cdot OH / O_2^- + Dye \rightarrow Degraded_{product} \quad (22)$$

The degradation pathway of MB dye can be seen in Fig. 9. First, the · *OH* attacked the sulfur-nitrogen conjugated system present in the MB dye molecules, to degrading it into B ((4-(N,N-dimethyl)-aniline) and C (2-amino-4-(N,N-dimethyl)-benzenesulfonic acid). After that, C is degraded to further produce F (2,4-hexadiene-1,6-diol), which cannot be degraded after. The series of reaction causes the other part of C to oxidized to form D (p-nitrobenzene-sulfonic acid), E (benzene-sulfonic acid) [36]. Similar reaction at B produces I(4-(N,N-dimethyl)-phenol) and J(hydro-quinone), which are then oxidized to G (malonic acid), H (propionic acid), CO_2 and H_2O. These results can be verified by the change in pH values from 6.35 to 6.64.

3.6. Recycling test

One of the primary problems for practical applications is the recycling of the produced composite. Ta-ZnO photocatalytic stability for MB degradation was therefore investigated. Five successive cycles of repeatability tests were carried out. The Ta-ZnO were collected after each run, cleaned several times with DI water and ethanol, and dried at 90°C for 18 hrs before the next cycle began. The slightly reduced decomposition is due to the intermediate adsorbed on the Ta-ZnO surface and the release of small amounts of Ta-ZnO into the solution during photocatalysis. For Ta-ZnO, cycles 1–4 took 105, 115, 110, and 120 mins respectively. The repeatability of synthesized photocatalyst against the MB dye degradation in shown in Fig. 8G. Table 2 presents the comparative assessment of ZnO based composites for photocatalytic degradation.

4. Conclusions

In this work, we present a potential approach for fabricating a bio-inspired tube using a nontoxic, biocompatible, and lotus-like microstructure replicated on PDMS materials coated with Ta-ZnO composite, which will undoubtedly provide a greater number of active sites for various applications. A real-time MB dye degradation is also monitored using the IoT technique by integrating a NodeMCU microcontroller board as a control center and a pH sensor as a tool for detecting the change in pH value of the MB dye. These lotus-like microstructure replicated on PDMS tubes were responsible for delivering a high surface-to-volume ratio for the formation of Ta-ZnO composite, as confirmed by SEM and EDS results. Further, this superhydrophobic (CA:168.0) bio-inspired polymeric platform was modified by optimizing the surface roughness and coating it with low-surface-energy Ta-ZnO NWs composites, paving the way for its to be utilized in "self-cleaning" water treatment facilities. The photocatalytic reaction of the Ta-ZnO NWs composite coated PDMS tube took 105 mins, which is faster than ZnO.

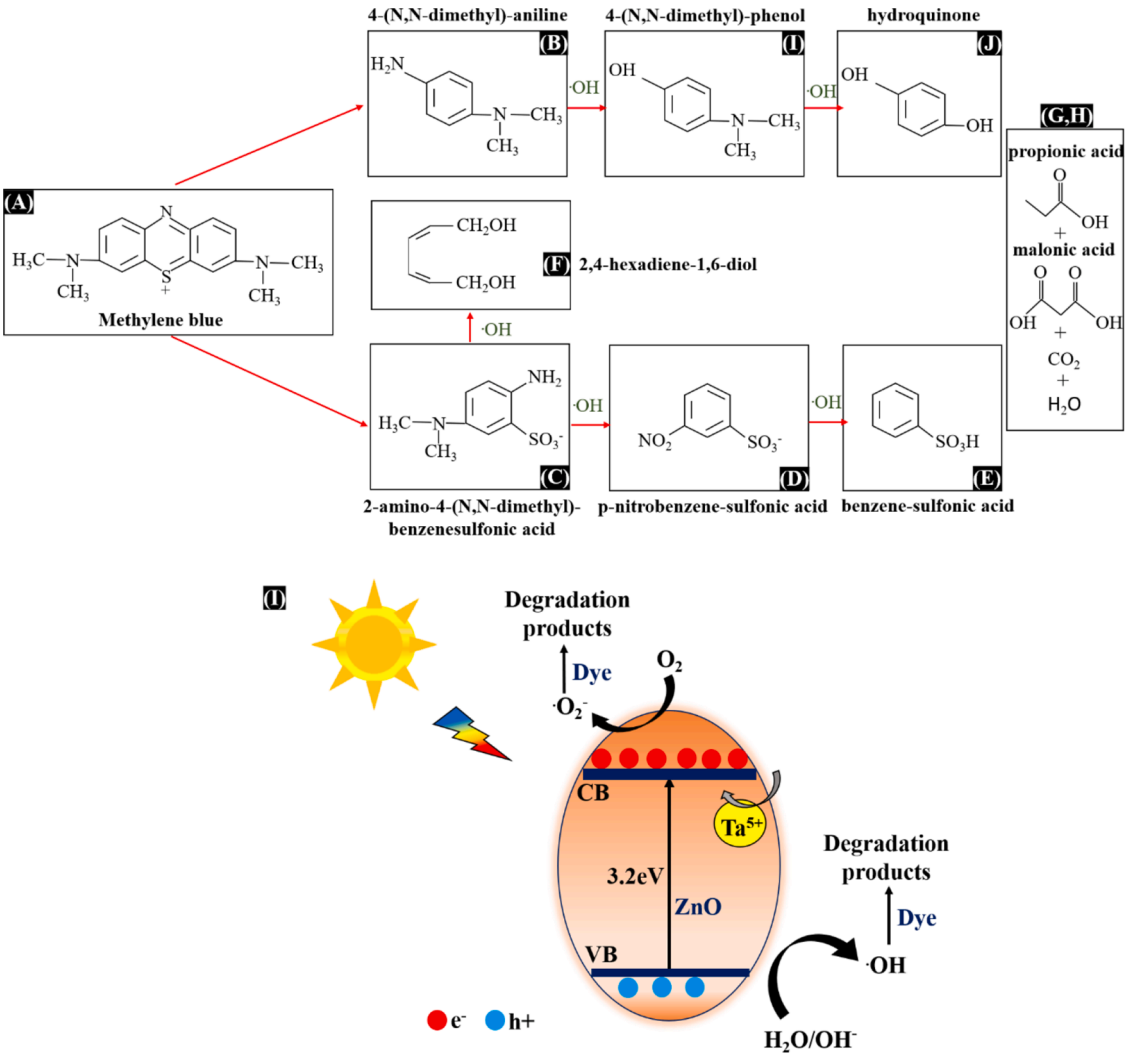

Fig. 9. (A-I) Possible degradation mechanisms of MB dye using Ta-ZnO composite.

Table 2
Previous work on the degradation of MB dye.

Photocatalyst	Exposing source	Irradiation time	Dye	Refs.
CA–CNT/TiO_2–NH_2	UV light	300 min	MB	[37]
Ni-doped CdS NPs	Sunlight	75 min	MB and MO	[38]
WO_3 nanoplate	UV light	105 min	MB	[39]
BiOI coating	UV light	150 min	MB	[40]
rGO/$CaSnO_3$ nanocomposite	UV light	150 min	MB	[41]
Ta-ZnO-PDMS	UV light	105 min	MB	Present work

These photocatalysts lead to "waste control using Ta-ZnO NWs composites," which opens up new possibilities for flexible and biocompatible environmental remediation platforms. Furthermore, this study might well assist researchers in better understanding the relationship between both synthesized composite structures and their photocatalytic degradation.

4.1. Funding information

The reported work is carried out with the help of partial financial support provided with the research seed grant (I/SEED/AKG/20190022) via affiliating institute (IIT Jodhpur), which was instrumental in completing the work.

4.2. Statements and declarations

Authors declare that there is no conflict among the contributing authors related to the financial or non-financial interests that are directly or indirectly related to the work submitted for publication.

Declaration of Competing Interest

The authors declare that they have no known competing financial interests or personal relationships that could have appeared to influence the work reported in this paper.

Data Availability

Data will be made available on request.

Acknowledgment

The corresponding author wishes to acknowledge the affiliating institute (IIT Jodhpur) for providing the research seed grant (I/SEED/AKG/20190022), which was instrumental in completing the work.

Author also wishes to acknowledge the SERB International Research Experience fellowship (SIR/2022/000188) provided by Science and Engineering Research Board, Department of Science and Technology, India.

Supplementary materials

Supplementary material associated with this article can be found, in the online version, at doi:10.1016/j.ceja.2022.100423.

References

[1] P.K. Rai, A. Gupta, Nanofunctionalized pulse-electroformed copper/graphene oxide tubular composite for efficient textile dye degradation under visible light irradiation, Appl. Nanosci. 2022 (2022) 1–16, https://doi.org/10.1007/S13204-022-02612-5.

[2] P.S. Chauhan, K. Kumar, K. Singh, S. Bhattacharya, Fast decolorization of rhodamine-B dye using novel V2O5-RGO photocatalyst under solar irradiation, Synth. Met. 283 (2022), https://doi.org/10.1016/J.SYNTHMET.2021.116981.

[3] P. Singh, R. Kant, A. Rai, A. Gupta, S. Bhattacharya, Materials science in semiconductor processing facile synthesis of ZnO /GO Nano Fl owers over si substrate for improved photocatalytic decolorization of MB dye and industrial wastewater under solar irradiation, Mater. Sci. Semicond. Process. 89 (2019) 6–17, https://doi.org/10.1016/j.mssp.2018.08.022.

[4] A. Gupta, S.S. Pandey, S. Bhattacharya, High aspect ZnO nanostructures based hydrogen sensing, in: 1536, 2013, pp. 291–292, https://doi.org/10.1063/1.4810215, 2013.

[5] A. Gupta, S.S. Pandey, M. Nayak, A. Maity, S.B. Majumder, S. Bhattacharya, Hydrogen Sensing Based On Nanoporous Silica-Embedded Ultra Dense ZnO Nanobundles, RSC Advances, 2014, pp. 7476–7482, https://doi.org/10.1039/c3ra45316b.

[6] A. Gupta, S. Bhattacharya, On the growth mechanism of ZnO nano structure via aqueous chemical synthesis, Appl. Nanosci 8 (2018) 499–509, https://doi.org/10.1007/s13204-018-0782-0.

[7] G. Verma, A. Gupta, Recent development in carbon nanotubes based gas sensors, J. Mater. Nanosci. 9 (1) (2022) 3–12.

[8] S. Chauhan, S. Singhal, S. Sirohi, Estimation of antimicrobial activity and nano-toxicity with optimized ZnO nanoparticles, Int. J. Adv. Res. Dev. Int. (2018) 1–6.

[9] G. Verma, P. Rai, J.G. Korvink, M. Islam, A. Gupta, Electrochemical processing and real-time degradation using Zno caterpillars photocatalyst for textile industry based wastewater recovery, SSRN Electron. J. (2022), https://doi.org/10.2139/SSRN.4203538.

[10] A. Gupta, G. Verma, Nanostructured Gas Sensors : Fundamentals, Devices, and Applications, 1st ed., 1, Jenny Stanford Publishing, 2023 https://doi.org/10.1201/9781003331230.

[11] G. Verma, A. Gupta, Superhydrophobic ZnO-Au nanocomposite over polydimethylsiloxane tubes for efficient photocatalytic dye degradation, Appl. Nanosci. (2022), https://doi.org/10.1007/S13204-022-02479-6.

[12] S. Chauhan, S. Singhal, S. Sirohi, Evaluation of biologically synthesized and characterized zinc oxide nanoparticles on propionibacterium acnes, Int. J. Creat. Res. Thoughts 6 (2) (2018) 333–341.

[13] X. Chen, T. Cao, M. Xue, H. Lv, B. Li, C. Zhang, Improved room temperature ionic conductivity of Ta and Ca Doped Li7La3Zr2O12 via a modified solution method, Solid State Ion. 314 (2018) 92–97, https://doi.org/10.1016/J.SSI.2017.11.027.

[14] G. Verma, A. Gupta, Sensing performance of room temperature operated MEMS gas sensor for ppb level detection of hydrogen sulfide: a review, J. Micromech. Microeng. (2022), https://doi.org/10.1088/1361-6439/AC82F8.

[15] J.Z. Kong, A.D. Li, X.Y. Li, H.F. Zhai, W.Q. Zhang, Y.P. Gong, H. Li, D. Wu, Photo-degradation of methylene blue using Ta-doped ZnO nanoparticle, J. Solid State Chem. 183 (6) (2010) 1359–1364, https://doi.org/10.1016/J.JSSC.2010.04.005.

[16] K. Chennakesavulu, M.M. Reddy, G.R. Reddy, A.M. Rabel, J. Brijitta, V. Vinita, T. Sasipraba, J.S Sreeramulu, Characterization and photo catalytic studies of the composites by tantalum oxide and zinc oxide nanorods, J. Mol. Struct. 1091 (2015) 49–56, https://doi.org/10.1016/J.MOLSTRUC.2015.02.052.

[17] X. Han, W. Wang, X. Ma, Adsorption characteristics of methylene blue onto low cost biomass material lotus leaf, Chem. Eng. J. 171 (1) (2011) 1–8, https://doi.org/10.1016/j.cej.2011.02.067.

[18] J. Lin, Y. Cai, X. Wang, B. Ding, J. Yu, M. Wang, Fabrication of biomimetic superhydrophobic surfaces inspired by lotus leaf and silver ragwort leaf, Nanoscale 3 (3) (2011) 1258–1262, https://doi.org/10.1039/C0NR00812E.

[19] X.M. Li, D. Reinhoudt, M. Crego-Calama, What do we need for a superhydrophobic surface? A review on the recent progress in the preparation of superhydrophobic surfaces, Chem. Soc. Rev. 36 (8) (2007) 1350–1368, https://doi.org/10.1039/B602486F.

[20] N. Sheshkar, G. Verma, C. Pandey, A. Kumar, S. Ankur, Enhanced thermal and mechanical properties of hydrophobic graphite - embedded polydimethylsiloxane composite, J. Polym. Res. 28 (403) (2021) 1–11, https://doi.org/10.1007/s10965-021-02774-w.

[21] G. Verma, N. Sheshkar, A. Gupta, C. Pandey, Recent trends of silicon elastomer-based nanocomposites and their sensing applications, J. Polym. Res. 29 (5) (2022) 1–26, https://doi.org/10.1007/s10965-022-03044-z.

[22] H.J. Biswal, P. Rout, P.R. Vundavilli, A. Gupta, Laser-assisted microhole fabrication in a flexible polymer substrate, Lasers Eng 49 (1) (2021) 3–20.

[23] G. Kumar Verma, M.Z Ansari, Design and simulation of piezoresistive polymer accelerometer, IOP Conf. Ser. Mater. Sci. Eng. (1) (2019) 561, https://doi.org/10.1088/1757-899X/561/1/012128.

[24] G. Verma, V. Kishnani, R.K. Pippara, A. Yadav, P.S. Chauhan, A. Gupta, Highly sensitive, ambient temperature CO sensor using tin oxide based composites, Sens. Actuators A Phys. 332 (2021), 113111, https://doi.org/10.1016/J.SNA.2021.113111.

[25] G. Verma, K. Mondal, A. Gupta, Si-based MEMS resonant sensor : a review from microfabrication perspective, Microelectronics J. 118 (2021) 1–64, https://doi.org/10.1016/j.mejo.2021.105210.

[26] G. Verma, A. Gupta, S. Bhattacharya, Internet of things (IoT)-assisted gas sensing technology. Gas Sensors, CRC Press, Boca Raton, 2022, pp. 287–302, https://doi.org/10.1201/9781003278047-19.

[27] P.S. Chauhan, A. Rai, A. Gupta, S. Bhattacharya, Enhanced photocatalytic performance of vertically grown ZnO nanorods decorated with metals (Al, Ag, Au, and Au-Pd) for degradation of industrial dye, Mater. Res. Express (5) (2017) 4, https://doi.org/10.1088/2053-1591/AA6D31.

[28] H.J. Biswal, A. Yadav, P.R. Vundavilli, A. Gupta, High aspect ZnO nanorod growth over electrodeposited tubes for photocatalytic degradation of EtBr dye, RSC Adv. 11 (3) (2021) 1623–1634, https://doi.org/10.1039/D0RA08124H.

[29] S. Marouf, A. Beniaiche, H. Guessas, A.M Azizi, Structural and optical properties of ZnO thin films deposited by dip coating method, Mater. Res. 20 (1) (2017) 88–95, https://doi.org/10.1590/1980-5373-MR-2015-0751.

[30] D. Richard, M. Romero, R. Faccio, Experimental and theoretical study on the structural, electrical and optical properties of tantalum-doped ZnO nanoparticles prepared via sol-gel acetate route, Ceram. Int. 44 (1) (2018) 703–711, https://doi.org/10.1016/j.ceramint.2017.09.232.

[31] S.D. Khairnar, V.S. Shrivastava, Facile synthesis of nickel oxide nanoparticles for the degradation of methylene blue and rhodamine B dye: a comparative study, J. Taibah Univ. Sci. 13 (1) (2019) 1108–1118, https://doi.org/10.1080/16583655.2019.1686248.

[32] S. Alkaykh, A. Mbarek, E.E. Ali-Shattle, Photocatalytic degradation of methylene blue dye in aqueous solution by $MnTiO_3$ nanoparticles under sunlight irradiation, Heliyon 6 (4) (2020) e03663, https://doi.org/10.1016/j.heliyon.2020.e03663.

[33] A. Khataee, M. Kiranşan, S. Karaca, S. Arefi-Oskoui, Preparation and characterization of ZnO/MMT nanocomposite for photocatalytic ozonation of a disperse dye, Turk. J. Chem. 40 (4) (2016) 546–564, https://doi.org/10.3906/KIM-1507-77.

[34] P. Senthil Kumar, P.S.A. Fernando, R.T. Ahmed, R. Srinath, M. Priyadharshini, A. M. Vignesh, A. Thanjiappan, Effect of temperature on the adsorption of methylene blue dye onto sulfuric acid–treated orange peel, Chem. Eng. Commun. 201 (11) (2014) 1526–1547, https://doi.org/10.1080/00986445.2013.819352.

[35] A.A. Babaei, S.N. Alavi, M. Akbarifar, K. Ahmadi, A. Ramazanpour Esfahani, B. Kakavandi, Experimental and modeling study on adsorption of cationic methylene blue dye onto mesoporous biochars prepared from agrowaste, Desalin. Water Treat. 57 (56) (2016) 27199–27212, https://doi.org/10.1080/19443994.2016.1163736.

[36] J. Lin, Z. Luo, J. Liu, P. Li, Photocatalytic degradation of methylene blue in aqueous solution by using ZnO-SnO2 nanocomposites, Mater. Sci. Semicond. Process. 87 (20) (2018) 24–31, https://doi.org/10.1016/j.mssp.2018.07.003.

[37] A. Salama, A. Mohamed, N.M. Aboamera, T.A. Osman, A. Khattab, Photocatalytic degradation of organic dyes using composite nanofibers under UV irradiation, Appl. Nanosci. 8 (1–2) (2018) 155–161, https://doi.org/10.1007/s13204-018-0660-9.

[38] M. Sankar, M. Jothibas, A. Muthuvel, A. Rajeshwari, S.J.S Jeyakumar, Optical and photocatalytic degradation of organic dyes by sol gel prepared Ni doped CdS nanoparticles, Surf. Interfaces 21 (2020), 100775, https://doi.org/10.1016/j.surfin.2020.100775.

[39] S.P. Gupta, H. Nishad, V. Magdum, P.S. Walke, High-performance supercapacitor electrode and photocatalytic dye degradation of mixed-phase WO3 nanoplates, Mater. Lett. 281 (2020), 128639, https://doi.org/10.1016/j.matlet.2020.128639.

[40] L. Hao, T. Liu, J. Yan, Y. Hu, F. Jiang, Q. Zhao, Y. Lu, X. Ping, Anodized BiOI coatings and their photocatalytic activity of organic dye degradation, Surf. Interfaces 20 (1038) (2020), 100562, https://doi.org/10.1016/j.surfin.2020.100562.

[41] G. Venkatesh, S. Prabhu, M. Geerthana, P. Baskaran, R. Ramesh, K.M. Prabu, Facile synthesis of RGO/$CaSnO_3$ nanocomposite as an efficient photocatalyst for the degradation of organic dye, Optik 212 (2020), 164716, https://doi.org/10.1016/j.ijleo.2020.164716 (Stuttg)January.